Linköping Studies in Science and Technology
Licentiate Thesis No. 1474

Deposition and Phase Transformations of Ternary Al-Cr-O Thin Films

Ali Khatibi

Linköping University
INSTITUTE OF TECHNOLOGY

LIU-TEK-LIC-2011:13
Thin Film Physics Division
Department of Physics, Chemistry, and Biology (IFM)
Linköping University
Linköping, Sweden

ISBN: 978-91-7393-210-3
ISSN: 0280-7971

Printed by LiU-Tryck
Linköping
February 2011

errors are not in the art, but in the artificers.

isaac newton

ABSTRACT

This thesis concerns the ternary Al-Cr-O system. $(Al_{1-x}Cr_x)_2O_3$ solid solution thin films with $0.6<x<0.7$ were deposited on Si(001) substrates at temperatures of 400-500 °C by reactive radio frequency magnetron sputtering from metallic targets of Al and Cr in a flow controlled Ar / O_2 gas mixture. As-deposited and annealed $(Al_{1-x}Cr_x)_2O_3$ thin films were analyzed by x-ray diffraction, elastic recoil detection analysis, scanning electron microscopy, transmission electron microscopy, and nanoindentation. $(Al_{1-x}Cr_x)_2O_3$ showed to have face centered cubic structure with lattice parameter of 4.04 Å, which is in contrast to the typical corundum structure reported for these films. The as-deposited films exhibited hardness of ~ 26 GPa and elastic modulus of 220-235 GPa. Phase transformation from cubic to corundum $(Al_{0.32}Cr_{0.68})_2O_3$ starts at 925 °C. Annealing at 1000 °C resulted in complete phase transformation, while no precipitates of alumina and chromia were observed. Studies on kinetics of phase transformation showed a two-step thermally activated process; phase transformation and grain growth with the apparent activation energies 213±162 and 945±27 kJ/mol, respectively.

PREFACE

This licentiate thesis is based on my PhD research studies in the Thin Film Physics Group at the Department of Physics, Chemistry and Biology (IFM) at Linköping University. The focus of my research is on the ternary oxide thin films of Al-Cr-O materials system. This investigation includes the deposition of $(Al_{1-x}Cr_x)_2O_3$ solid solution thin films followed by annealing studies. Financial support to my work is provided by the Swedish Research Council (VR).

INCLUDED PAPERS

PAPER I

Face-Centered Cubic $(Al_{1-x}Cr_x)_2O_3$

A. Khatibi, J. Palisaitis, C. Höglund, A. Eriksson, P. O. Å. Persson, J. Jensen, J. Birch, P. Eklund, L. Hultman

Thin Solid Films 519 (2011) 2426–2429

PAPER II

Kinetics of Phase Transformation in fcc-$(Al_{1-x}Cr_x)_2O_3$ Thin Films

A. Khatibi, J. Lu, J. Jensen, P. Eklund, L. Hultman

In Manuscript

ACKNOWLEDGEMENTS

I would like to thank…

... *Lars Hultman*, my supervisor, for his scientific and strategic supervision, and for giving me the chance to pursue my career in a group with such scientific spirit.

... *Per Eklund*, my co-supervisor, for the scientific and experimental supervision.

... *Inger, Kalle, Thomas, and the entire group staff* for their valuable help.

... *all my friends and colleagues* in the Thin Film, Nanomaterials, and Plasma groups for their kind friendship. They have had an irreplaceable role in increasing my Swedish language knowledge.

... and last but not least, *my wife and all other family members* for standing beside me during all steps of my studies.

TABLE OF CONTENTS

1. INTRODUCTION

1.1 THIN FILM TECHNOLOGY

It is hard to find a product which does not benefit from thin film technology. Thin films are nowadays used from less than one atomic monolayer up to few micrometers, depending on the desired purpose. One main reason to apply thin films to the surface of a bulk material, or substrate, is that the bulk material can not provide all the properties that we desire for a specific application. By applying a thin film, we can profit from both the bulk and surface properties, simultaneously. Thin films are applied to several products that we use in our daily life. For instance: decorative coatings to give a better finish and glaze to the furniture and household appliances, heat-filtering coatings applied to glass windows to preserve the indoor temperature of buildings, wear-, corrosive-, or heat-resistant coatings used in industry for high-temperature applications, e.g. jet turbines, or watery environments, e.g. ships, coatings applied to hard drives in electronic industries, and so on. These are just a few examples out of thousands of applications for thin films.

1.2 BACKGROUND

This work is associated with thin films of a ternary-oxide materials system consisting of chromium, aluminum and oxygen. Binary oxides of chromia (Cr_2O_3) and alumina (Al_2O_3) have been investigated for decades in both industry and academia. Chromia is the hardest known oxide (29.5 GPa). Cr_2O_3 thin films are well-studied regarding the deposition and properties [1-5]. Alumina is also a famous binary oxide known to form many polymorphs, the thermodynamically stable one of which is α-alumina, also known as corundum [6-9] and well known to the public as the gemstones sapphire and ruby. During recent years, there have been efforts to study the coexistence of chromia and alumina in thin films. This is motivated by their similar structural properties; they are in the same crystallographic space group [10]. These efforts have been either to use corundum-structured chromia as a template to assist the low-temperature growth of α-alumina or to form a homogenous solid solution of Al-Cr-O thin films. Regarding the former case, promising results have been reported showing that α-

chromia templates have assisted the deposition of α-alumina at low temperatures. Deposition of α-alumina at low temperatures is not possible/practical, which is due to the presence of several metastable phases such as γ, θ and κ. In contrary, deposition of α-chromia thin films can take place at relatively low temperatures, which in part, helps the formation of α-alumina thin films at low deposition temperatures (see [11-13]). To fulfill the latter case (i.e., deposition of Al-Cr-O solid solution thin films), different methods have been employed including cathodic arc evaporation [14-17] and magnetron sputtering [18,19]. According to the pseudo-binary phase diagram of Al_2O_3-Cr_2O_3, synthesis of Al-Cr-O solid solutions is challenging at low deposition temperatures. This is due to the presence of a *miscibility gap* at low temperatures. However, deposition of thin films takes place at non-equilibrium conditions while the extraction of phase diagrams are based on the equilibrium conditions. This is explained in more details in the following chapter.

1.3 OBJECTIVES

The first objective of this work is to synthesize Al-Cr-O solid solution thin films. The second objective is to determine what phase transformations occur during annealing of the deposited Al-Cr-O solid solution thin films.

1.4 OUTLINE OF THE THESIS

The following chapter starts with an overview on the binary oxides of Al_2O_3 and Cr_2O_3, though the focus will be mostly on the ternary system of Al-Cr-O. In this part, the pseudo-binary phase diagram of Al_2O_3-Cr_2O_3 is explained. In addition, concepts such as *solid solution, miscibility gap, spinodal decomposition, and nucleation and growth* will be discussed followed by a part devoted to *rhombohedral* and *face centered cubic* crystal structures. Chapter three describes deposition of films by *physical vapor deposition* with a focus on reactive magnetron sputtering. Chapter four is about the techniques and methods by which the deposited films are characterized. At the end, an outline of the plans for the continuation of this study is presented.

2. BINARY AND TERNARY OXIDES

2.1 BINARY OXDIES OF CHROMIA AND ALUMINA

Chromia (Cr_2O_3) and alumina (Al_2O_3) and are two of the most well-known ceramic materials on earth. There have been many studies devoted to these two binary oxide materials systems during the past decades. Chromia is the hardest among the known oxides (29.5 GPa). It has a wide range of applications in corrosion protection, wear resistance, electronics and optics [1-5]. Alumina has also been a very interesting materials system for materials scientists. In addition to have a vast range of applications similar to the aforementioned ones for chromia, it has been crystallographically well-studied due to its *polymorph* nature. A compound is called polymorph if it takes different crystal structures, but is unique in chemical formula. Alumina has several polymorphs such as α, γ, κ, θ of which, α-alumina is thermodynamically stable at room temperature [6,20]. Chromia and α-alumina are identical in crystal structure.

2.1.1 CORUNDUM CRYSTAL STRUCTURE

The crystal structure of α-alumina and α-chromia is known as *corundum*. In this structure, oxygen atoms form a semi-hexagonal close packed (hcp) sublattice in which aluminum atoms are placed in two-thirds of the octahedral sites [21]. The top view of corundum structure (figure 2.1.b) shows the semi-hcp structure of oxygen atoms. The side view of structure shows the presence of 18 oxygen and 12 aluminum atoms. It is important to note that the primitive cell of α-alumina has a rhombohedral lattice with a basis that consists of 6 O and 4 Al atoms, but it is more convenient to show the structure as hexagonal shown in figure 2.1.

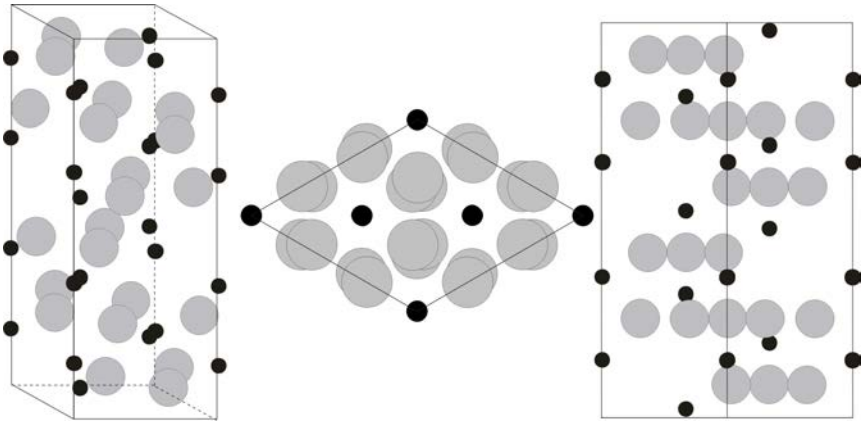

(a) (b) (c)

Figure 2.1 (a) perspective, (b) top, and (c) side views of corundum crystal structure in which big and small circles represent oxygen and metal (Al in alumina and Cr in chromia), respectively.

2.2 THE TERNARY Al-Cr-O SYSTEM

In this section, the binary phase diagram of Al_2O_3-Cr_2O_3 is explained which shows the conditions in which chromium, aluminum, and oxygen can coexist as either solid solution or phase separated.

2.2.1 THE PSEUDO-BINARY PHASE DIAGRAM OF Al_2O_3-Cr_2O_3

Figure 2.2.a shows the pseudo-binary phase diagram of Al_2O_3-Cr_2O_3 at the thermodynamically equilibrium conditions [22]. According to this phase diagram, the area which contains the solid solutions of Al-Cr-O alloys (marked by *$(Al,Cr)_2O_3(ss)$* in figure 2.2.a) is limited by the solidus line from top. In this area, the solid solutions of Al-Cr-O exist for the whole range of compositions down to the temperatures of ~1250 °C. Below this temperature and for the compositions with molar fraction of Cr_2O_3<0.8, the solid solution area is limited by a dashed line (or full line at higher pressures). This line is the boundary of *miscibility gap* area and separates the solid solution from the phase separated of Al-rich and Cr-rich regions. A miscibility gap occurs if two elements or phases form an endothermic solid solution, i.e., when the difference in the enthalpy of system before and after the mixture, ΔH_{mix}, has a positive value (i.e., $\Delta H_{mix} > 0$). We know that the Gibbs free energy, ΔG, of a system is defined as $\Delta H - T\Delta S$ in which, ΔS is

the difference in entropy. At high temperatures, $T\Delta S_{mix}$ is a large term and therefore, ΔG_{mix} becomes negative meaning that solution is thermodynamically stable. At low temperatures, $T\Delta S_{mix}$ is small and therefore, ΔG_{mix} becomes positive for a certain range of compositions; meaning that solid solution is not anymore thermodynamically stable. In a miscibility gap, there is a region in which the Gibbs free energy curve has a negative curvature, i.e., $d^2G/dx^2 < 0$ (Figure 2.2.b). This region is called *chemical spinodal* and upon cooling, one-phase alloys with a composition falling in this region may undergo a phase transformation named *spinodal decomposition*. Spinodal decomposition is an *up-hill* process in which the alloy components move toward the higher concentrations [23]. Spinodal decomposition in the Al_2O_3-Cr_2O_3 system was observed by Schultz and Stubican for a powder-metallurgy prepared (55 mol% Al_2O_3-45 mol% Cr_2O_3) solid solution of α-$(Al_{1-x}Cr_x)_2O_3$ annealed at temperature of 800 °C [24].

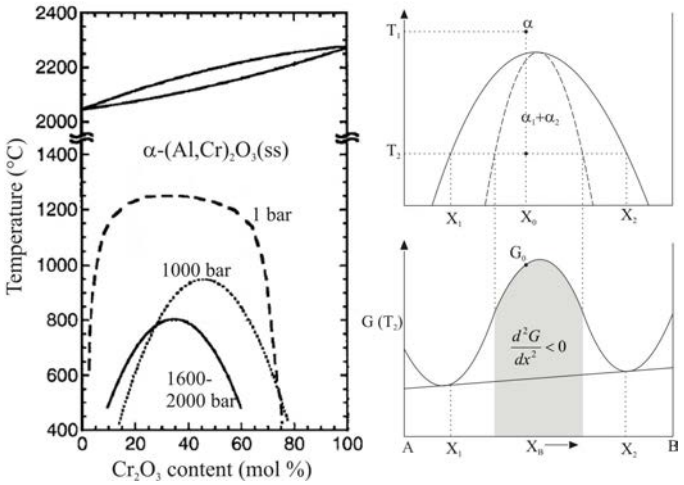

(a) (b)

Figure 2.2 (a) Binary phase diagram of Al_2O_3-Cr_2O_3 (adopted from Ref. 22) and (b) Gibbs free energy of an alloy falling in a spinodal region (redrawn from Ref. 25). The single phase region at 1 bar is marked by α-$(Al_{1-x}Cr_x)_2O_3$(ss) in (a). By increasing the pressure, the miscibility gap moves toward the lower temperatures.

3. THIN FILM DEPOSITION

There are several methods for the deposition of thin films. Most of these methods are categorized in one of the four families of (1) physical, (2) chemical, (3) hybrid (physical-chemical), and (4) patterning techniques [26]. For a comprehensive list, see Refs. 27-28. In this thesis, the focus is on physical vapor deposition (PVD) aimed at Magnetron sputtering.

One of the main advantages of PVD over other deposition methods such as chemical vapor deposition (CVD) is the low range of temperatures in which the deposition processes take place. In chemical methods, thin film deposition is done by the formation of chemical bonds between the deposition species and the dangling bonds of the substrate surface's atoms. This process occurs through chemical reactions at high temperatures (e.g., 1000 °C) which is not suitable for heat-sensitive substrates. Moreover, such high temperatures results in build up of residual stress in the films during cooling which can ease the generation of cracks. Instead, in PVD methods, due to the absence of chemical reactions at the vicinity of substrate, deposition takes place at relatively low temperatures which makes it suitable for variety of applications; from microelectronics to hard coatings.

3.1 PHYSICAL VAPOR DEPOSITION

In the deposition of thin films by PVD method, the first step is to transform the deposition source (called *target*) from its solid or liquid state to the gas phase. This is done by physical ejection of target species. One of the primary ways to do that is the evaporation of deposition species by heating up the target. This technique is called *thermal evaporation*. One alternative to thermal evaporation is to *"kick out"* the deposition material from a solid target. This process is named *sputtering* and is carried out by the bombardment of target surface with floating positively charged ions in plasma (e.g. Ar^+). In addition to thermal evaporation and sputtering, there are other methods to eject the target materials, e.g., *cathodic arc evaporation*. In this method, a low-voltage, high-current plasma discharge builds arc spots on the target surface which results in the evaporation of target material [29].

3.2 SPUTTER DEPOSITION

3.2.1 BASICS OF SPUTTERING

Figure 3.1.a shows a schematic drawing of a typical sputter deposition system along with its three notable elements; cathode, anode, and plasma. The target is the cathode with a negative potential applied. When sputtering gas (e.g. argon) flows into the chamber, the few positively charged ions which are initially present in the gas accelerate toward the cathode and hit the target. As a result of that, different species such as sputtered atoms, secondary electrons, reflected ions, and neutrals are emitted from the target surface (figure 3.2.b). The generated secondary electrons hit the gas atoms which cause the creation of more ions. These ions are again attracted by the negative potential of cathode and bombard the target. This cycle repeats which results in a stable plasma.

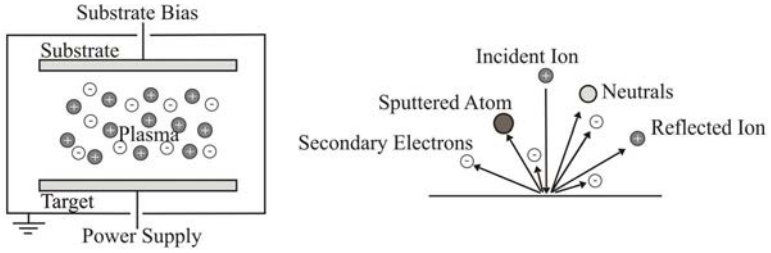

(a) (b)

Figure 3.1 Schematic illustration of (a) a typical magnetron sputtering deposition system, and (b) processes occurring on the surface of target during a sputtering process.

3.2.2 WHAT IS PLASMA?

Plasma is the fourth state of matter next to solid, liquid, and gas. By definition, plasma is a collection of charged particles that move in all directions randomly and is on the average (or equivalent) electrically neutral [30,31]. These charged particles are electrons and positive ions. Electrons have much higher mobility than ions, since they are much lighter, which results in accumulation of electrons on the anode (substrate). It causes the plasma to obtain a positive potential and consequently every other object in plasma, e.g., the substrate, obtains negative potential. Finally, the substrate repels the further coming electrons, which results in an equal flux of electrons and ions. The potential of this surface is known as *floating potential*, V_f [32]. This potential causes the

bombardment of substrate with positively charged ions. The level of substrate bombardment can be increased if it is *biased* with a bias voltage. A negative bias voltage attracts more positive ions toward the substrate, i.e., the substrate (growing film) is bombarded with highly energetic ions. This results in the transfer of energy to the deposition species providing higher mobility for them. This is a determining parameter to have a film with higher density. Figure 3.2 shows the plasma ignited in the deposition system used in this study.

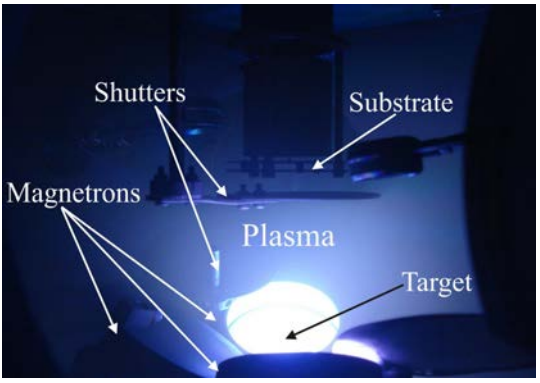

Figure 3.2 The deposition process seen through a glass window in the chamber's wall. Plasma, 2-inch-magnetrons (cathode) and substrate (anode) are marked in the image.

3.3 MAGNETRON SPUTTERING

The simple sputtering processes suffer from the need for a quite high working pressure (in a range of a few Pa) in order to sustain the discharge. The reason for such a need is the ability of generated secondary electrons to escape from the vicinity of target toward the anode. Working in such high pressure is a drawback in the process of thin film growth since it might introduce a high level of impurities to the growing film. Moreover, the deposition rate is low, which is the direct consequence of low sputtering rate of target. These problems led to the invention of a complementary process in which the electrons are confined to the vicinity of target by using a magnetic field; a method named *magnetron sputtering*.

3.3.1 BASICS OF THE MAGNETRON

Since the introduction of magnetron sputtering, different types of magnetrons have been developed and used in research and industry, e.g., cylindrical, planar, and rotating cylindrical magnetrons. The magnetron used in this study is a cylindrical one in which a series of magnets sit right in the back side of the target plate in a way that two poles are formed. One pole is in the center of target by a single column of magnets while the other pole forms by a ring of magnets sitting in the circumference of target (figure 3.3.a). The magnetic lines formed in between the two poles do not let the secondary electrons escape from the neighborhood of target. As a result, the number of collisions between the secondary electrons and gas atoms increases resulting in higher level of gas ionization. Therefore, target is bombarded by additional number of ions and sputtering rate increases, resulting in significant raise of deposition rate at substrate [33].

Depending on the design of the magnetron, the strength of the central magnet can be the same as or different from the outer ring of magnets. If they are the same, the magnetron is called *balanced* (figure 3.3.b) in which all of the magnetic lines from outer magnets end up in the central magnet or vice versa (although in practice, no magnetron is completely balanced). If the strengths of the magnets are not the same in the center and the outer ring, the magnetron is called *unbalanced* and is the type used in this study (figure 3.3.c). One main difference between the balanced and unbalanced magnetrons is the effect of their magnets' arrangement on how the plasma is spread in the chamber between the target and substrate. In a balanced magnetron, the plasma is confined to the area close to target (< 6 cm) and therefore, it is dense. This is often not good because if the film growth takes place within this distance, the growing film is subjected to a lot of ion bombardment in such dense plasma resulting in many defects such as buried positive ions, inconsistency of crystal structure, interstitials, etc., in the film. On the other hand, the substrates out of this distance will experience a very low deposition rate due to the low plasma density. To solve these problems, using an unbalanced magnetron can help because the plasma is less dense and the deposition rate is higher where the substrate is placed [33,34].

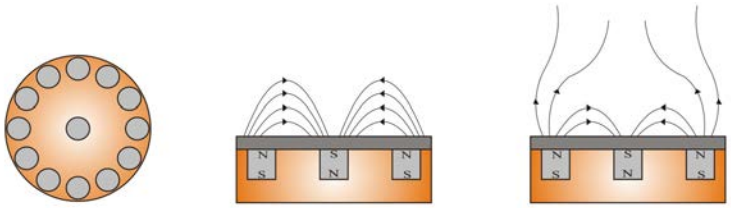

(a) (b) (c)

Figure 3.3 Schematic drawings of a top view from the arrangement of magnets placed in the back of target plate (a), and the side views of the magnetic lines in a balanced (b) and unbalanced (c) cylindrical magnetron.

There are different methods to power the magnetrons of which we can name, direct current (DC), radio frequency (RF), pulsed DC, and high power impulse magnetron sputtering (HIPIMS). The film depositions in this thesis have been performed by using RF powered magnetrons, so we neglect the other methods in the rest of discussions.

3.3.2 RADIO-FREQUENCY (RF) MAGNETRON SPUTTERING

For the deposition of electrically non-conducting films such most oxides and many nitrides, DC magnetron sputtering is not always the best choice and instead other magnetron sputtering methods such as pulsed-DC or RF are usually employed. The reason is the insulating layer which forms during a reactive sputtering process (see section 3.3.3) on top of the target if the process is carried out in poisoned mode (see section 3.3.3.1). This layer makes a lot of trouble for the continuation of process. To avoid the formation of such a layer, RF-powered magnetrons have been employed. As we already read in section 3.2.1, target always functions as a cathode in basic sputtering process, while it is not the case here. In RF magnetron sputtering, cathode and anode are changeable and for very short cycles, target functions as anode which cause the removal of insulating layer. By doing so, the process can continue [35,36]. There are also a number of drawbacks with RF sputtering such as lower deposition rates and complexity of the system which requires impedance-matching networks and expensive power supplies. [37]. Figure 3.4 shows the sputtering system - called *Jessie* – along with the control and RF-maching units stationed in the laboratory of IFM department at Linköping university. For further details of chamber and system set up, see [38].

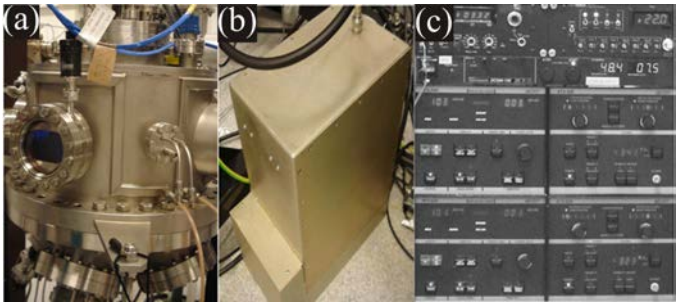

Figure 3.4 Images of (a) the deposition chamber used in this study, (b) RF matching unit, and (c) control unit of the system.

3.3.3 REACTIVE SPUTTERING

To deposit compound films such as oxides or nitrides, the magnetron sputtering process can take place by sputtering from either a compound target in an ambient of pure sputtering gas (e.g. argon) or an elemental metallic target in an ambient of the reactive and sputtering gases (e.g. oxygen or nitrogen in argon). The former has not shown to be an efficient process due to low deposition rates (for insulating materials). The latter method is known as *reactive sputtering* which is the choice in this study to deposit the ternary Al-Cr-O oxide thin films. Over the years, many good studies and reviews on reactive sputtering process are performed which are mostly devoted to the reaction of target and reactive gas (e.g. see [39, 40]). This is crucial because the amount of reactive gas flow has a direct consequence on the stoichiometry of films, deposition rates, etc. It is explained by *hysteresis* effect.

When a reactive gas (here oxygen) enters the chamber with low flows, it reacts with all free surfaces such as chamber walls and substrate and form oxides with the materials sputtered from target(s). Therefore, it does not experience any change in its partial pressure until a certain flow (point A in figure 3.5). At this point, all the possible surfaces for getter pumping are covered with oxide compounds. Therefore, any further increase in the oxygen flow causes the formation of an insulating layer of oxide on top of the target leading to a rapid increase in the partial pressure of oxygen. This is the beginning of a transition region from a fully metallic target at point A to a fully poisoned target at point B. At this point (B), the whole target surface is covered with a layer of oxide which has a

quite lower sputtering rate than metallic target; leading to a remarkable drop in deposition rate. The region in between points A and B is called *transition* region in which one would like to perform the reactive sputtering process. By using *partial pressure control* system, it is fully possible to sustain the deposition process in the transition region. Further increase in the oxygen flow at point B results in increasing of partial pressure in a linear relation with its flow. Upon the decreasing of oxygen flow, as shown in figure 3.5, partial pressure of oxygen does not return to its low value right away after point B and remains large enough for the formation of oxide layer until point C is reached. At this point, the oxide layer on top of the target is broken through which results in a higher sputtering yield from the metallic areas on target. More sputtered materials means more getter pumping of oxygen and therefore, decrease in the partial pressure of oxygen to point D. The loop formed by the points A, B, C, and D is called “hysteresis loop” and shows the complex behavior of reactive gas partial pressure vs. flow in a reactive sputtering process [41].

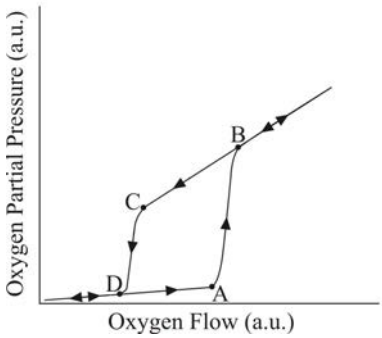

Figure 3.5 Schematic drawing of hysteresis loop which takes place during a reactive sputtering process.

4. CHARACTERIZATION OF FILMS

Different instruments and techniques are used to determine the crystal structure, elemental composition, and mechanical properties of the films. The ones which are used in this thesis are *x-ray diffraction* (XRD), *elastic recoil detection analysis* (ERDA), *scanning electron microscopy* (SEM), *transmission electron microscopy* (TEM), and *nanoindentation.*

4.1 X-RAY DIFFRACTION

X-rays are electromagnetic waves which have wavelengths of the order of 10^{-10} meters (= 1 Ångström). It makes them able to probe the interatomic spacings and determine crystal structure. Moreover, it is a non-destructive technique [42].

The principle of x-ray diffraction is based on scattering. It means that when x-rays enter condensed matter, they scatter in all directions. Scattering of electrons make constructive and destructive interferences. When constructive interference happens, intensities add and show up as peaks (in Bragg angles) while in the case of destructive interference, x-rays cancel each other. This phenomenon was first introduced mathematically by W. L. Bragg in 1912 and is named Bragg's law:

$$2d \sin \theta = n\lambda, \tag{4.1}$$

in which θ and λ are the scattering angle and the wavelength of the x-rays, respectively. d is the spacing of the measured set of planes. In this thesis, the Cu K_α (λ = 1.54 Å) is used as the x-ray source to study the films in two different modes; $\theta/2\theta$ scan and pole figures.

4.1.1 $\theta/2\theta$ SCAN

In the symmetric $\theta/2\theta$ scans, the incoming and outgoing beams make equal angles with respect to the film surface during the measurement. Therefore, the scattering vector is always normal to the film surface and as a result, only planes parallel to the surface are probed. In this way, by probing the desired sample for an adequate range of 2θ angles, the intensity and location of the peaks (compared to the XRD databases) are employed for

determination of phase in the measured sample. In phase determination by using θ/2θ scans, it is helpful to check for the absence of *forbidden peaks*. In each crystal structure (except simple cubic), there are some families of crystallographic planes which are not allowed to give diffraction in the θ/2θ diffractograms of their corresponding measured samples. This is due to the *structure factor, S*, which is identical for each crystal structure. The value of structure factor determines the conditions for which, the crystallographic planes can or can not give diffraction in a specific crystal structure. For example, in an fcc structure, those crystallographic planes that have their hkl Miller indices as a mixture of odd and even numbers (e.g., (100)) will not give any diffraction because for these planes, S = 0 (for details of calculations, see Ref. 43). Therefore, these peaks are not present in the θ/2θ diffractogram and are known as forbidden peaks. Along with the other characterization methods such as TEM, forbidden peaks are used here for the determination of crystal structure (see Paper I)

4.1.2 POLE FIGURES

In a symmetric θ/2θ scan, only the planes which are parallel to the film surface will give diffraction, while the film might contain grains with different orientations as well, e.g. in a polycrystalline film. To investigate that, XRD is used for texture analysis. The result of this measurement is a stereographic projection of the orientations that are present in a measured film at a fixed 2θ angle. This technique has been employed in this thesis to aid the determination the crystal structure of the as-deposited films. A typical pole figure is shown in figure 4.1 and belongs to $(Al_{0.31}Cr_{0.69})_2O_3$ film deposited at 400 °C (Paper I). This pole figure has been measured at 2θ = 65.25° which corresponds to the location of (220) plane in an fcc film with a lattice constant of 4.04 Å. The pole figure shows a ring of diffraction at ψ = 45°, which is the angle between (200) and (220) planes.

4.2 ELASTIC RECOIL DETECTION ANALYSIS

The elemental composition of films was determined by elastic recoil detection analysis (ERDA). In this technique, heavy projectiles ions such as Cl, Ni, I, or Au at high range of energies like MeV (in this thesis, 40 MeV $^{127}I^{9+}$) are incident on the film surface. As these projectiles penetrate into the film (max. ~ 1 μm), they knock out the atoms that

are lighter in mass. The emitted atoms can then detected by, e.g., a time-of-flight energy (ToF-E) detector (the case in this thesis). In ToF-E detectors, the recoiled atoms will travel in between two foils before they reach the detector for energy measurement. By measuring the time (t) they need to pass the distance (L) between the foils and their energy (E), their masses can be determined by using the following equation.

$$m_i = \frac{2E_i t^2}{L^2}, \tag{4.2}$$

Figure 4.2 shows the elemental composition of the $(Al_{0.52}Cr_{0.48})_2O_3$ film deposited at 500 °C, which is measured by ERDA.

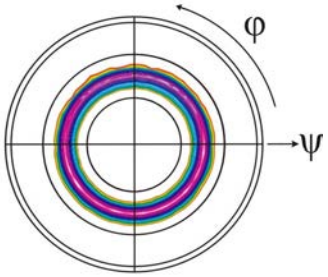

Figure 4.1 Pole figure measured at 2θ = 65.25° from a $(Al_{0.31}Cr_{0.69})_2O_3$ film deposited at 400 °C. φ and ψ are azimuth and tilt angles, respectively. The pole figure shows a diffraction ring at ψ = 45°, which corresponds to the angle between (200) and (220) planes.

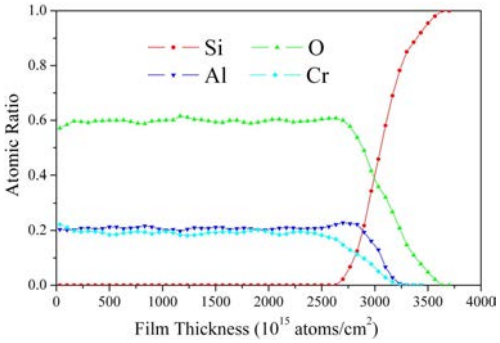

Figure 4.2 ERDA depth profile of the $(Al_{0.52}Cr_{0.48})_2O_3$ film deposited at 500 °C.

4.3 ELECTRON MICROSCOPY

Electron microscopes are widely used in characterization of thin film. Optical microscopes have the limitation of wavelength (~ 550 nm) and the best resolution provided by them is approximately 200 nm, while due to the short-wavelength nature of electrons (~ 2.5 pm at 200 kV accelerating voltage[44]) as the used beam in electron microscopes, it is possible to gather information in the scale of interatomic distances. In comparison to XRD, electron microscopy is sometimes a more beneficial method. For instance, a crystalline film with very small grains (e.g. < 3 nm) will show up as amorphous in XRD due to very small cross sections provided by the small grains, while electron microscopy might show the crystallinity. Another example is recording a diffraction pattern, which can take quite long time in XRD, while it takes less than a second in TEM.

4.3.1 SCANNING ELECTRON MICROSCOPY

Scanning Electron Microscopy is a technique in which the sample surface is scanned by an electron beam. As a result of interaction between sample surface and electron beam, different signals are emitted such as secondary and backscattered electrons, x-rays, and Auger electrons. Among all, secondary electrons have lower energy and can escape only from near the sample surface and therefore, they are used to study the topography of surfaces in SEM. Moreover, SEM is used to study the cross section of samples in which the microstructure, level of defects and porosity, and film morphology can be investigated. In addition to all, cross-section SEM is used in this thesis to determine the thicknesses of Al-Cr-O deposited films. Figure 4.3 shows a cross sectional SEM micrograph of $(Al_{0.31}Cr_{0.69})_2O_3$ film in which the columnar structure of the films in out-of-plane orientations is shown. The film thickness is ~ 2 µm.

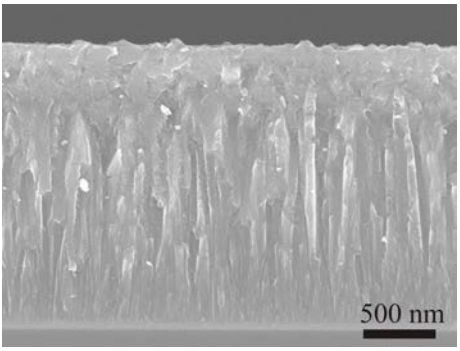

Figure 4.3 Cross sectional SEM micrograph of a $(Al_{0.31}Cr_{0.69})_2O_3$ film showing its columnar structure.

4.3.2 TRANSMISSION ELECTRON MICROSCOPY

In transmission electron microscopy, a beam of electrons passes through a very thin sample, which results in emission of several different signals, similar to the ones in SEM introduced in section 4.3.1. One difference between SEM and TEM is the range of accelerating voltages which they work on. SEMs work in the range of 5–20 kV while for conventional TEMs, this number is in the range of 100 to 400 kV. Such high operating voltages provide the TEM instruments with higher energetic electrons than SEMs.

There are many useful applications in TEMs which make it an invaluable technique in characterization of thin films. Some of them are used in this thesis and will be explained in the following sections.

The main feature of TEM samples is that they should be really thin (~50 nm) and that is why sample preparation is an important stage. The reason for having such a thin sample is to avoid plural scattering (> 1 time) and multiple scattering (>20 times) when the electron is traveling through the sample, although plural scattering is inevitable. When the number of electron scattering increases, it gets more and more difficult to interpret the electron behavior and consequently the images and electron diffractions.

4.3.2.1 HIGH RESOLUTION TRANSMISSION ELECTRON MICROSCOPY

High resolution transmission electron microscopy (HRTEM) is a technique of TEM, which allows crystal lattice-resolved imaging and therefore, is suitable for studying the

materials in nanoscales. In HRTEM, the mechanism by which an image forms is *phase contrast*. When the high-energy electron wave emit through a TEM sample, the electrons may be affected by the sample's crystal structure. It means that either they continue their path along the same direction as they entered the sample (the beam's direction) and leave it undeviated or they diffract as a result of "scattering" from the crystallographically ordered atoms in the sample lattice planes. The corresponding electron waves for these two conditions are named as transmitted and diffracted waves, respectively. Since transmitted and diffracted waves are different in phase, their interference produces intensity variations, which is detected by the microscope. These intensity variations are then used to determine the location of atoms in the formed HRTEM image. Such an image is shown in figure 4.4.b for the $(Al_{0.31}Cr_{0.69})_2O_3$ film.

To achieve the best possible resolution in HRTEM, a very accurate alignment of the beam and the sample is needed, although it is not perfectly possible due to two main reasons: 1) the presence of imperfections in the electromagnetic lenses (i.e., astigmation and chromatic and spherical aberrations), and 2) the lack of knowledge we have in interpretation of the atomic models [45].

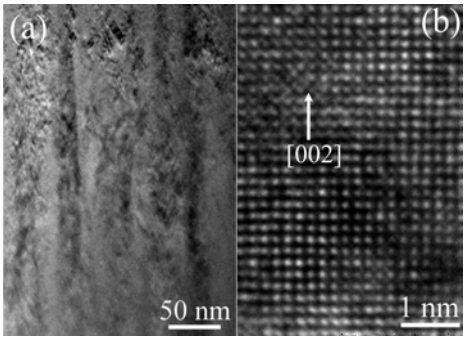

Figure 4.4 (a) low magnification TEM and (b) HRTEM images of a $(Al_{0.31}Cr_{0.69})_2O_3$ film deposited at 400°C.

4.3.2.2 ELECTRON DIFFRACTION

Electron diffraction is a method in which the reciprocal lattice is imaged, similar to the diffraction pattern obtained in XRD. However, there are differences as well. Electron

diffraction patterns in TEM are formed as a result of Coulomb interactions of electrons with the nucleus of atoms, while x-rays diffraction patterns are generated when x-rays are scattered against the core electrons of atoms in the measured sample. Another difference is the time needed for recording of patterns by electrons and x-rays. Recording an electron diffraction pattern can takes place in less than a second in TEM, while recording a diffraction pattern in XRD can takes several hours. Also, a main benefit of electron diffraction over other method such as x-ray is the low wavelength of electrons (in the range of pm) which makes it possible to verify very small volumes in the specimen [46].

In TEM, electron diffraction patterns form in the back focal plane of the objective lens. There are two techniques for recording an electron diffraction pattern in TEM; selected area electron diffraction (SAED) and convergent beam electron diffraction (CBED). In SAED, the illumination of sample is performed by using a parallel beam of electron. Also, using a selected area aperture on the back focal plane of the objective lens (diffraction plane) makes it possible to record the electron diffractions from areas as small as ~ 100-200 nm, providing crystallographic information from each grain in an e.g., polycrystalline material. In CBED, on the other hand, the electron beam illuminates the sample at its ultimately possible convergence angle and therefore, electron diffraction from a very small area is obtained. In CBED mode, the electron diffraction pattern is in form of circles instead of solid focused spots. CBED patterns are used for determination of point and space groups [47]. In SAED patterns, the shape of recorded electron diffraction pattern can help to determine if the specimen is an amorphous, single crystal or a polycrystalline one. Also, by aligning the central beam along a zone axis and measuring the distance of diffraction from the center of pattern, the diffractions can be named based with the Miller indices of the planes from which their respective diffraction have come. Here, this is performed for $(Al_{0.31}Cr_{0.69})_2O_3$film deposited at 400 °C (figure 4.5)

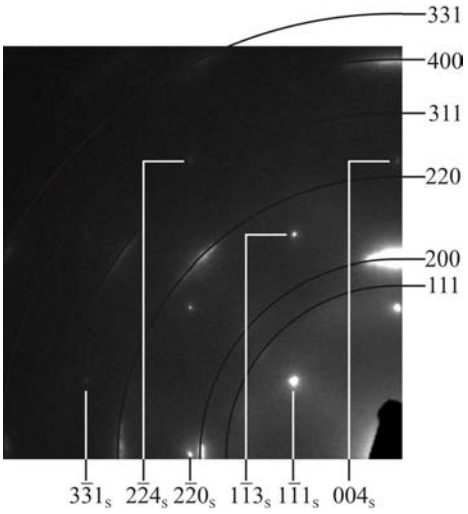

Figure 4.5 Electron diffraction pattern for the TEM image showed in figure 4.4.a. Diffraction spots from the Si substrate are labeled with "S" as subscript.

4.3.2.3 SCANNING TRANSMISSION ELECTRON MICROSCOPY

Scanning transmission electron microscopy (STEM) is combination of SEM and TEM techniques. The reason is that to form an STEM image, the high-voltage electron beam (characteristic of TEM) scans the surface (characteristic of SEM) at several small steps. What makes STEM different from conventional TEM is the very small beam used in this technique. Here, the electron beam size is less than 10 nm (in ideal case < 1 nm) while in TEM mode, the beam size is usually around 1μm and even bigger. In STEM mode, the incoherent-elastic electrons which are scattered at angles above 10° are detected by a high-angle annular dark field (HAADF) detector to form the image. STEM images have better contrast in both BF and DF than TEM images, although they are noisier and have poorer resolution in BF mode. Furthermore, the contrast mechanism is mass-thickness contrast, meaning that the heavier the atoms in the film, the more scattered the electrons will be. In this thesis, STEM technique is used in combination with other techniques such as electron energy loss spectroscopy (EELS) and energy dispersive x-ray spectroscopy (EDX) by employing very small probe sizes of 1-5 nm to study the compositional variations in very small areas. For example, line scan

measurements in TEM EDX (section 4.4) are used to determine the compositional ratios at sub-grain boundaries in Al-Cr-O solid solution thin films (see the low-magnification TEM image in figure 4.4.a).

4.4 ENERGY DISPERSIVE X-RAY SPECTROSCOPY

Energy Dispersive X-ray spectroscopy (EDX) is one of the analytical methods of electron microscopy in which the emitted x-ray from the sample is detected by a semiconductor detector. In EDX detectors, three elements of H, He, and Li are not detected by EDX technique due to their low-energy x-rays.

X-rays are characteristic to the elements from which they are emitted. This is the result of filling the empty place of a core electron - which is ejected by scattered electron beam – by an electron from outer shells. During this process, the excited atom will come back to its ground state and characteristic x-ray will be emitted. In x-ray spectroscopy, the count of emitted x-rays will be recorded vs. their corresponding energy and therefore, the chemical mapping of the scanned area (mostly in STEM mode) will be achieved. In this thesis (see Paper I), this method is used to indicate the presence of solid solution of ternary oxide by showing the signals of elemental composition in in-plane and out-of-plane orientations (figure 4.6).

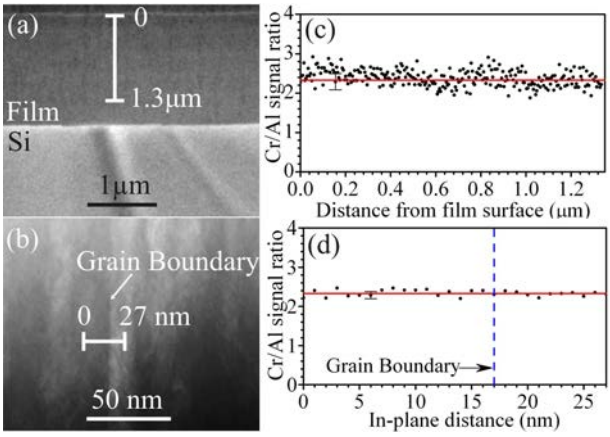

Figure 4.6 TEM EDX measurements of the stoichiometric $(Al_{0.31}Cr_{0.69})_2O_3$ film deposited at 400 °C along (a) and (c) out-of-plane orientation with step size of 5 nm, and (b) and (d) in-plane orientation with step size of 1 nm. The measurement error bars are indicated in (c) and (d). The Cr/Al signal-intensity ratio is normalized to the compositional.

4.5 NANOINDENTATION

In this study, hardness, H, and reduced elastic modulus, E_r, are measured by employing the nanoindentation method followed by data interpretation using Oliver and Pharr method [45]. To perform the measurement, a diamond tip (in this thesis, Berkovich indent) indents the film by increasing the load at several small steps until the maximum load, P_{max}, is achieved. The maximum indentation depth, h_{max}, takes place at maximum load and is the determining factor for the film hardness measurement. Also, the slope of the unloading curve (indicated as S in figure 4.7) is used to measure the reduced elastic modulus, E_r. E_r is then related to Young's modulus (i.e., E) by a relationship in which Poisson's ratio is included. P_{max} and h_{max} are shown schematically in figures 4.7. h_f is the plastic deformation formed as a result of indentation process.

In nanoindentation test, the choice of P_{max} is critical for the measurement results and can affect the values of H and E considerably. A determining parameter which should be taken into consideration for choosing the right value of P_{max} is the thickness of the film. It is important because a nanoindentation test on an identical film with different thicknesses can result in different values of H and E, though P_{max} is the same in all. This is due to the surface and substrate effects at low and high loads, respectively. In principle, the right P_{max} in nanoindentation test is the one for which, the indention depth is independent of the applied load. In this thesis, to determine P_{max}, a measurement was performed on each film in which, the applied load was increased from low loads (~ 8 mN) to high loads (~ 37 mN) in several steps (dP = 0.5 mN). For most of the films, P_{max} is set to 25-28 mN. The average values for H and E_r for Al-Cr-O solid solution films were determined as 26 GPa and 220-235 GPa, respectively (Paper I).

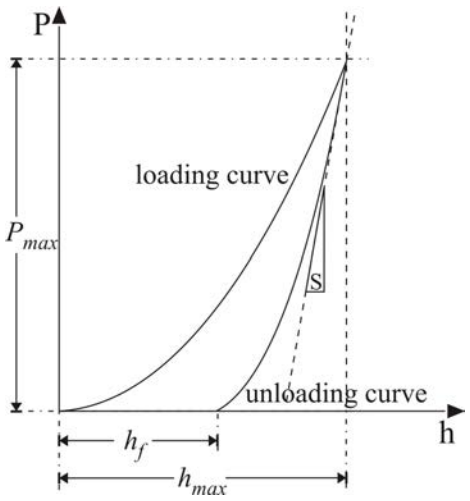

Figure 4.7 Schematic representation of loading-unloading curves (redrawn from Ref. 45) used in Oliver-Pharr method to interpret the nanoindentation data.

5. CURRENT RESEARCH AND FUTURE PLANS

This work has been focused on (1) the deposition of $(Al_{1-x}Cr_x)_2O_3$ solid solution thin films by reactive radio frequency magnetron sputtering and (2) annealing studies of the deposited films, as presented in Papers I and II, respectively.

For the continuation of my PhD studies, I plan to explore the range of compositions to stabilize cubic and hexagonal Al-Cr-O films. To do this, I will employ the cathodic arc deposition. With such as-deposited solid solutions, I will test the hypothesis of age hardening in Al-Cr-O system.

This study will then continue by changing the ternary system of Al-Cr-O to the quaternary Al-Cr-O-N system. Introduction of nitrogen can increase the toughness of the synthesized coatings by the effects from covalent bonds in an otherwise ionic structure of the oxide system. On the other hand, Al-Cr-O-N films may be mechanically hard and at the same time, less brittle with respect to Al-Cr-O films. The deposition of $(Al_{1-x}Cr_x)O_{1-y}N_y$ thin films will be performed in an industrial cathodic arc deposition. In this setup, alloyed targets with different Al/Cr ratio will be employed in an atmosphere of O_2/N_2. As a preliminary work for this research plan (not included in this thesis), five series of $(Al_{1-x}Cr_x)O_{1-y}N_y$ films with $0 \leq y \leq 1$ have been deposited.

To investigate the properties of ternary oxides in other related oxide systems, my plan is to substitute the Cr in Al-Cr-O by a similar element in electronic and ionic structure, which can be Ce or Gd.

6. SUMMARY OF PAPERS

The main novelty of the work presented in this thesis is the discovery of a new crystal structure for $(Al_{1-x}Cr_x)_2O_3$ solid solution thin films (Paper I). The previous works on this materials system have reported the formation of $(Al_{1-x}Cr_x)_2O_3$ solid solution thin films with *corundum* structure, while here I find *face centered cubic (fcc)* crystal structure for the $(Al_{1-x}Cr_x)_2O_3$ films with $0.6<x<0.7$ deposited at substrate temperature of 400 ºC. This finding is shown in $\theta/2\theta$ and texture measurements by x-ray diffraction (XRD) and further confirmed by high resolution transmission electron microscopy (HRTEM) and selected area electron diffraction (SAED). The lattice parameter of the fcc structure was determined as 4.04 Å by both Bragg's calculation based on $\theta/2\theta$ XRD and HRTEM observations. I suggest in this paper that the $(Al_{1-x}Cr_x)_2O_3$ solid solution thin films have atomic basis of non-1:1 NaCl with 33% vacancies in metallic Al/Cr sites. The measured values for hardness and elastic modulus are 26 GPa and 220-235 GPa, respectively.

In addition, the thermal stability of the fcc-$(Al_{0.32}Cr_{0.68})_2O_3$ solid solution thin films was investigated (Paper II) by annealing in ambient air in a quartz-wall furnace at temperatures of 500-1100 ºC for 2-10 h. Based on XRD diagrams HRTEM images, and SAED patterns , a phase transformation from fcc to corundum is observed at 925 ºC by the emerging peaks from $(11\bar{2}3)$ and $(11\bar{2}6)$-oriented grains. The kinetics and activation energy of this phase transformation is determined by the Johnson-Avrami-Mehl (JAM) transformation equation. This study showed that the phase transformation from fcc phase to corundum phase in Al-Cr-O materials system is a thermally activated two-step process; phase transformation and grain growth with apparent activation energies of 213±162 and 945±27 kJ/mol, respectively.

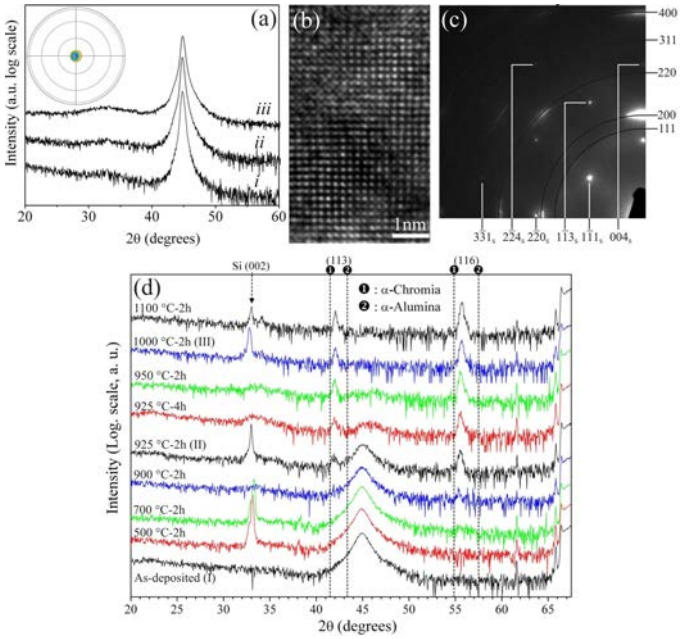

Figure 6.1 (a) XRD diagrams and pole figure (inset), (b) HRTEM image, and (c) SAED pattern of the $(Al_{1-x}Cr_x)_2O_3$ films with $0.6<x<0.7$ (Paper I). (d) XRD θ/2θ scans from a $(Al_{0.32}Cr_{0.68})_2O_3$ film annealed to different states (Paper II). I,II, and III represent three samples of the $(Al_{0.32}Cr_{0.68})_2O_3$ film, which are as-deposited, annealed at 925 ºC, and annealed 1000 ºC, respectively.

REFERENCES

[1] F. Luo, X. Pang, K. Gao, H. Yang, and Y. Wang, "*Role of deposition parameters on microstructure and mechanical properties of chromium oxide coatings*", Surf. Coat. Technol. 202 (2007), pp. 58–62.

[2] P. Hones, M. Diserens, and F. Lévy, "*Characterization of sputter-deposited chromium oxide thin films*", Surf. Coat. Technol. 120-121 (1999), pp. 277–283.

[3] B. Bhushan, "*Characterization of R.F.-sputter-deposited chromium oxide films*", Thin Solid Films 73 (1980), pp. 255-265.

[4] A. Khanna, D. G. Bhat, and E. A. Payzant, "*Growth and characterization of chromium oxide thin films prepared by reactive ac magnetron sputtering"*, J. Vac. Sci. Technol. A 24 (2006), pp. 1870-1877.

[5] X. Pang, K. Gao, F. Luo, H. Yang, L. Qiao, Y. Wang, and A. A. Volinsky, , "*Annealing effects on microstructure and mechanical properties of chromium oxide coatings"*, Thin Solid Films 516 (2008), pp. 4685–4689.

[6] I. Levin and D. Brandon, "*Metastable alumina polymorphs: crystal structures and transition sequences*", J. Am. Ceram. Soc. 81 (1998), pp. 1995 -2012.

[7] K. Koski, J. Hölsä, and P. Juliet, "*Deposition of aluminium oxide thin films by reactive magnetron sputtering*", Surf. Coat. Technol. 116 (1999), pp. 716–720.

[8] R. Cremer, K. Reichert, D. Neuschütz, G. Erkens, and T. Leyendecker, "*Sputter deposition of crystalline alumina coatings*", Surf. Coat. Technol. 163-164 (2003), pp. 157–163.

[9] F. Fietzke , K. Goedicke, and W. Hempel, "*The deposition of hard crystalline Al_2O_3 layers by means of bipolar pulsed magnetron sputtering*", Surf. Coat. Technol. 86-87 (1996), pp. 657-663.

[10] M. Ristić, S. Popović, and S. Musić, "*Structural properties of the system Al_2O_3- Cr_2O_3*", Mater. Lett. 16 (1993), pp. 309-312.

[11] P. Eklund, M. Sridharan, M. Sillassen, and J. Bøttiger, "*α-Cr_2O_3 template-texture effect on α- Al_2O_3 thin-film growth*", Thin Solid Films 516 (2008), pp. 7447–7450.

[12] P. Jin, S. Nakao, S.X. Wang, and L.M. Wang, "*Localized epitaxial growth of a-Al_2O_3 thin films on Cr_2O_3 template by sputter deposition at low temperature*", Appl. Phys. Lett. 82 (2003), pp. 1024-1026.

[13] J. M. Andersson, Zs. Czigány, P. Jin, and U. Helmersson, "*Microstructure of a-alumina thin films deposited at low temperatures on chromia template layers*", J. Vac. Sci. Technol., A 22 (2004), pp. 117-121.

[14] J. Ramm, M. Ante, T. Bachmann, B. Widrig, H. Brändle, and M. Döbeli, "*Pulse enhanced electron emission (P3e™) arc evaporation and the synthesis of wear resistant Al-Cr-O coatings in corundum structure*", Surf. Coat. Technol. 202 (2007), pp. 876–883.

[15] J. Ramm, M. Ante, H. Brändle, A. Neels, A. Dommann, and M. Döbeli, "*Thermal stability of thin film corundum-type solid solutions of $(Al_{1-x}Cr_x)_2O_3$ synthesized under low-temperature non-equilibrium conditions*", Adv. Eng. Mater. 9 (2007), pp. 604-608.

[16] D. Levchuk , H. Bolt, M. Döbeli, S. Eggenberger, B. Widrig, and J. Ramm, "*Al-Cr-O thin films as an efficient hydrogen barrier*", Surf. Coat. Technol. 202 (2008), pp. 5043–5047.

[17] L. A. Vieira, M. Döbeli, A. Domman, E. Kalchbrenner, A. Neels, J. Ramm, H. Rudigier, J. Thomas, and B. Widrig, "*Approaches to influence the microstructure and the properties of Al-Cr-O layers synthesized by cathodic arc evaporation*", Surf. Coat. Technol. 204 (2010), pp. 1722–1728.

[18] M. Witthaut, R. Cremer, K. Reichert, and D. Neuschütz, "*Preparation of Cr_2O_3-Al_2O_3 Solid Solutions by Reactive Magnetron Sputtering*", Mikrochim. Acta 133 (2000), pp. 191-196.

[19] K. Pedersen, J. Bøttiger, M. Sridharan, M. Sillassen, and P. Eklund, "*Texture and microstructure of Cr_2O_3 and $(Cr,Al)_2O_3$ thin films deposited by reactive inductively coupled plasma magnetron sputtering*", Thin Solid Films 518 (2010), pp. 4294–4298.

[20] W. H. Gitzen, "*Alumina as a ceramic material*", American Ceramic Society (1st edition, 1970), p. 23.

[21] M. Barsoum, "*Fundamentals of Ceramics*", McGraw-Hill (1st edition, 1997), pp. 63-66.

[22] M. Fujita, K. Inukai, S. Sakida, T. Nanba, J. Ommyoji, A. Yamaguchi, and Y. Miura, "*Sintering of Al_2O_3-Cr_2O_3 powder prepared by sol-gel process*", J. Soc. Mater. Sci. Japan **56** (2007), pp. 526-530.

[23] D. A. Porter, and K. E. Easterling, "*Phase Transformation in Metals and Alloys"*, Chapman & Hall (2nd edition, 1995), pp. 308-314.

[24] A.H. Schultz and V.S. Stubican, "*Seperation of Phases by Spinodal Decomposition in the Systems Al_2O_3-Cr_2O_3 and Al_2O_3-Cr_2O_3-Fe_2O_3 "*, J. Am. Ceram. Soc. 53 (1970) pp. 613-616.

[25] D. A. Porter, and K. E. Easterling, "*Phase Transformation in Metals and Alloys"*, Chapman & Hall (2nd edition, 1995), p. 309.

[26] J. L. Vossen, and W. Kern, "*Thin film processes I*", Academic press (1st edition, 1978), p. 3.

[27] P. M. Martin, "*Handbook of deposition technologies for films and coatings*", Elsevier (3rd edition, 2010), pp. 10-12.

[28] J. L. Vossen, and W. Kern, "*Thin film processes I*", Academic press (1st edition, 1978), p. 4.

[29] I. G. Brown, "*Cathodic arc deposition of films*", Annu. Rev. Mater. Sci. 28 (1998), pp. 243-269.

[30] M. A. Lieberman, and A. J. Lichtenberg, "*Principles of plasma discharges and materials processing*", John Wiely & Sons (2nd edition, 2005), p. 7.

[31] M. Ohring, "*Materials science of thin films*", Academic press (2nd edition, 2002), p. 147.

[32] J. L. Vossen, and W. Kern, "*Thin film processes II*", Academic press (1st edition, 1991), pp. 14-15.

[33] P.J. Kelly, and R.D. Arnell, "*Magnetron sputtering: a review of recent developments and applications*", Vacuum 56 (2000), pp. 159-172.

[34] M. Ohring, "*Materials science of thin films*", Academic press (2nd edition, 2002), pp. 227-229.

[35] J. L. Vossen, and W. Kern, "*Thin film processes II*", Academic press (1st edition, 1991), pp. 24-32.

[36] P. M. Martin, "*Handbook of deposition technologies for films and coatings*", Elsevier (3rd edition, 2010), pp. 277-278.

[37] M. Ohring, "*Materials science of thin films*", Academic press (2nd edition, 2002), pp. 211-216.

[38] D.H. Trinh, M. Ottosson, M. Collin, I. Reineck, L. Hultman, and H. Högberg, " *Nanocomposite Al_2O_3-Zr_2O_3 thin films grown by reactive dual radio-frequency magnetron sputtering*", Thin Solid Films 516 (2007), pp. 4977–4982.

[39] W.D. Sproul, D.J. Christie, and D.C. Carter, "*Control of reactive sputtering processes*", Thin Solid Films 491 (2005), pp. 1 – 17.

[40] I. Safi, "*Recent aspects concerning DC reactive magnetron sputtering of thin films: a review*", Surf. Coat. Technol. 127 (2000), pp. 203-219.

[41] D. Depla, and S. Mahieu, "*Reactive Sputter Deposition*", Springer (1st edition, 2008), pp. 131-133.

[42] M. Birkholz, "*Thin Film Analysis by X-Ray Scattering*", Wiley-VCH (1st edition,2006), p. 1.

[43] C. Kittel, "*Introduction to Solid State Physics*", John Wiely & Sons (8th edition, 2004), p. 72.

[44] D. B. Williams, C. B. Carter, "*Transmission Electron Microscopy*", Springer (1996), p. 6.

[45] W. C. Oliver, G. M. Pharr, "*An improved technique for determining hardness and elastic modulus using. load displacement sensing indentation experiments*", J. Mater. Res., 7 (1992), pp. 1564-1583.

[46] D. B. Williams, C. B. Carter, "*Transmission Electron Microscopy*", Springer (1996), pp. 179-189.

[47] L. A. Bendersky and F. W. Gayle, "*Electron Diffraction Using Transmission Electron Microscopy*", J. Res. Nat. Inst. Stand. Technol. 106 (2001), pp. 997-1012.